Theory of Forward Stimulated Brillouin Scattering in Dual-Mode Single-Core Fibers

P. St. J. Russell, D. Culverhouse, and F. Farahi

Abstract—**Recently, stimulated Brillouin scattering in a forward direction (FSBS) in a dual-mode single-core optical fiber was reported for the first time. Frequency shifts on the order of 17 MHz were seen in fiber supporting LP_{01} and LP_{11} modes at 514.5 nm. The phenomenon is examined here in more detail, and the governing differential equations of the three-wave parametric process (involving laser pump, Brillouin signal, and acoustic flexural-wave phonon) are derived and solved. FSBS is possible because although the overlap integral between a flexural fiber mode and the light is small, the phonon lifetime is much longer than in conventional SBS. FSBS may also be the first example of a nonlinear effect which is enhanced by *increasing* the optical mode area at constant pump power.**

I. Introduction

THIS paper presents a detailed analysis of a new nonlinear effect observed recently for the first time by the authors [1]—intermodal stimulated Brillouin scattering in a forward direction (FSBS) in dual-mode (DM) fibers. FSBS differs from the guided acoustic-wave Brillouin scattering reported by Shelby *et al.* [2] in being based on genuine collinear phase matching between three distinct guided waves and displaying a stimulated threshold. The recent growth of interest in DM optical fibers for a variety of nonlinear switching and modulation schemes [3]–[8] owes its origin to the long interaction lengths that are possible in fiber waveguides, and to the interesting new experimental possibilities offered by a structure that supports two nondegenerate copropagating modes at the same optical frequency. These factors give DM fiber waveguides unique advantages over bulk optics for the study of new nonlinear optical phenomena. Some recent examples include all-optical switching in twin-core [3], Hi–Bi [4], and periodically rephased mismatched dual-core fibers [5], [6]. DM fibers have also been used to form acoustooptical frequency shifters [7]–[9] by exciting flexural waves on them and matching the acoustic wavelength to the intermodal beat length. Detailed analyses [8], [10] of these devices are of direct relevance to the present study of FSBS; intermodal beating (between the Brillouin and pump light) excites (via electrostriction) a flexural wave that, in turn, couples power between the modes.

This paper is organized as follows. In Section II, the underlying physical intuitive basis for FSBS is discussed. Intermodal beating between the LP_{01} and LP_{11} modes at different frequencies is treated in Section III, and an expression is found for the induced electrostrictive moment. The wave equation for low-frequency flexural waves is obtained in Section VI, and the electrostrictive source term is incorporated. Intermodal coupling via flexural microbending is analyzed in Section V, and the full set of differential equations describing the parametric interaction, normalized to power, it obtained in Section VI. In Section VII, approximate analytical expressions for the Brillouin gain are found and solutions are obtained. These results are discussed in Section VIII, the evolution of the power in the three waves with propagation distance is modeled (by numerical integration of the equations), and threshold power levels for BSBS and FSBS are calculated. Conclusions are drawn in Section IX.

Manuscript received June 22, 1990; revised January 2, 1991.

P. St. J. Russell was with the Physics Laboratory, University of Kent, Canterbury CT2 7NR, England. He is now with the Optoelectronics Research Centre, University of Southampton, Southampton SO9 5NH, England.

D. Culverhouse is with the Physics Laboratory, University of Kent, Canterbury CT2 7NR, England.

F. Farahi was with the Physics Laboratory, University of Kent, Canterbury CT2 7NR, England. He is now with the Department of Physics, University of North Carolina, Charlotte, NC 28223.

IEEE Log Number 9143425.

II. Physical Basis: Momentum and Energy Conservation

Two basic conservation laws must be obeyed for Brillouin scattering to occur. The first is conservation of energy:

$$\hbar\omega_L = \hbar\omega_B + \hbar\Omega \tag{2.1}$$

and the second is conservation of momentum:

$$\boldsymbol{k}_L = \boldsymbol{k}_B + \boldsymbol{K} \tag{2.2}$$

where ω_L, ω_B, and Ω are the radian frequencies and $\boldsymbol{k}_L$, $\boldsymbol{k}_B$, and $\boldsymbol{K}$ are the wavevectors of the pump laser, Brillouin, and acoustic waves. In addition to these conservation laws, there must exist two *nondegenerate* normal modes at the pump optical frequency. In a *single-mode* optical fiber, only two modes satisfying this condition are available—the backward and forward propagating ones; hence, the Brillouin signal appears in the backward direction (leading to backward stimulated Brillouin scattering—BSBS). In a DM fiber, by contrast, the LP_{01} and LP_{11} modes satisfy this condition, making permissible the generation of an intermodal SBS signal in the forward direction.

The physical process underlying FSBS is a circular loop of cause and effect. Spontaneous acoustic phonons (flexural waves in this case) generate, through the strain-optical effect, weak traveling refractive index gratings in the fiber core. Those phonons whose wavelength $\Lambda_F = v_F/f_F$ (where v_F is their phase velocity and f_F is their frequency) equals the intermodal beat period L_b will weakly Bragg scatter light between the fiber modes, causing Stokes and anti-Stokes frequency conversion from the pump into the Brillouin signals. The pattern of moving interference fringes generated by intermodal frequency mixing of the Stokes and pump modes has points of constructive interference that alternate back and forth across the fiber core (see Fig. 1). This creates, via electrostriction, a moving, periodically reversing moment wave whose wavelength matches that of the original spontaneous phonon. If, in addition, the spatial

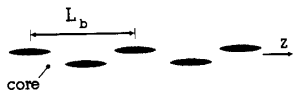

Fig. 1. Schematic of intermodal beating. Constructive interference between the LP_{01} and LP_{11} modes occurs on alternate sides of the core at a spatial beat period $L_b = 2\pi/|k_L - k_B|$. During FSBS, this pattern moves, its wavelength and phase velocity matching those of a flexural acoustic mode of the fiber.

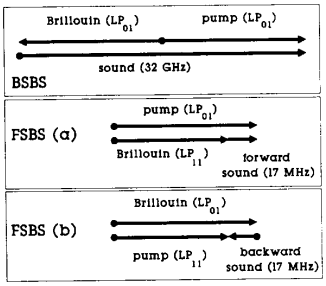

Fig. 2. Wavevector conservation in normal backscattered SBS, $LP_{01} \rightarrow LP_{11}$ FSBS, and $LP_{11} \rightarrow LP_{01}$ FSBS. The arrows represent (schematically) the wavevectors, pointing parallel to the phase velocities of each wave. Note that in FSBS (b), the acoustic phase velocity is negative.

registration of the moment wave relative to the acoustic wavefronts is correct, the spontaneous acoustic wave will experience gain. This, in turn, increases the scattering strength into the Brillouin wave, thus closing the loop of cause and effect. If the electrostrictive gain over the phonon coherence length is greater than the acoustic loss, then FSBS can occur; both the acoustic and the Brillouin waves will experience exponential gain.

In FSBS, the direction of the phonon wave depends on whether the frequency down-conversion is $LP_{01} \rightarrow LP_{11}$ or vice versa (Fig. 2). Unlike backward SBS where the threshold power depends strongly on the laser linewidth, in FSBS, this condition is considerably relaxed, permitting a multifrequency laser pump to be used. This is because the pump and Brillouin waves propagate along exactly the same optical path, and hence can maintain mutual coherence over very long lengths of fiber.

III. Intermodal Beating: Induced Electrostrictive Moment

The superposition of pump and Brillouin signals (each in a different linearly polarized fiber mode) yields a total electric field:

$$E_{\text{tot}}(r, \phi, z, t) = \tfrac{1}{2}\{e_B(r, \phi)A_B(z) \exp\{-j(k_B z - \omega_B t)\} + e_L(r, \phi)A_L(z) \exp\{-j(k_L z - \omega_L t)\} + \text{c.c.}\} \tag{3.1}$$

where A_B and A_L are the electric field amplitudes and $e_B(r, \phi)$ and $e_L(r, \phi)$ are the dimensionless transverse mode profiles, equal either to $e_{01}(r)$ or $e_{11}(r, \phi)$, depending on circumstances (see Fig. 3 for the coordinate system). It is clear that this compound field will contain intermodulation components at frequency $\Omega = \omega_L - \omega_B$, with associated wavevector $K = k_L - k_B$. If K equals the wavevector at frequency Ω of a flexural fiber mode, these components will phase match to it. Acoustic gain is then possible via electrostriction, and FSBS may occur. To

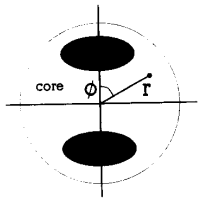

Fig. 3. Coordinate system for evaluation of the overlap integral $Q \approx r_{eq}/2a$. The elliptical shaded regions represent the intermodal beat pattern.

treat the effect of electrostriction, it is necessary to find the energy stored per unit volume ($W = \epsilon E_{\text{tot}}^2/2$) and convert it into a change in pressure [11]. Selecting those components of W that travel forward (for $LP_{01} \rightarrow LP_{11}$ conversion) at velocity Ω/K, one obtains

$$W = \frac{\epsilon}{4} e_{11}(r, \phi)e_{01}(r)A_B^* A_L \cdot \exp\{-j(Kz - \Omega t)\} + \text{c.c.} \tag{3.2}$$

For a uniaxial strain s along the fiber axis, electrostriction is governed by the parameter [8]

$$\frac{\partial \epsilon_r}{\partial s} = 2n^2(1 - \chi) \tag{3.3}$$

where $\epsilon_r = \epsilon/\epsilon_o$ and $\chi = 0.22$ for fused silica, yielding $\partial\epsilon_r/\partial s = 3.3$. This leads to an axial component of electrostrictive stress Δp in the form

$$\Delta p(r, \phi, z, t) = \epsilon_o \frac{\partial \epsilon_r}{\partial s} \frac{1}{4}\{e_{11}(r, \phi)e_{01}(r)A_B^*(z)A_L(z) \cdot \exp\{-j(Kz - \Omega t)\} + \text{c.c.}\}. \tag{3.4}$$

The stress wave in (3.4) is periodic, with a wavelength equal to the beat length between the LP_{01} and LP_{11} modes. When the background dc electrostrictive stress field is superimposed, regions of high stress alternate with z between the upper and lower hemispheres of the core (as already depicted in Fig. 1). The induced electrostrictive driving moment may be calculated as follows:

$$M_d(z, t) = \int\int \Delta p(r, \phi) r^2 \cos\phi \, d\phi \, dr \tag{3.5}$$

where the integral is over the fiber cross section (Fig. 3). This yields finally

$$M_d(z, t) = \epsilon_o \frac{\partial \epsilon_r}{\partial s} \frac{a}{4}\{Q A_{\text{eq}} A_B^*(z)A_L(z) \cdot \exp\{-j(Kz - \Omega t)\} + \text{c.c.}\} \tag{3.6}$$

where a is the fiber radius and the overlap integral Q is given by

$$Q = \frac{1}{aA_{\text{eq}}} \int_{r=0}^{a} \int_{\phi=0}^{2\pi} e_{01}(r)e_{11}(r, \phi) r^2 \cos\phi \, dr d\phi \tag{3.7}$$

and e_{01} and e_{11} are defined such that the equivalent modal area (spot size) is

$$A_{\text{eq}} = \int\int e_{11}^2(r, \phi) r dr d\phi = \int\int e_{01}^2(r) r dr d\phi. \tag{3.8}$$

The overlap integral may be shown to be given approximately by $Q \approx r_{eq}/2a$ where $r_{eq} = \sqrt{(A_{eq}/\pi)}$ is the mode spot radius.

IV. Low-Frequency Flexural-Wave Equation with Drive Term

Low-frequency flexural waves obey the wave equation [12]

$$\rho A \frac{\partial^2 y}{\partial t^2} + EI \frac{\partial^4 y}{\partial z^4} = 0 \tag{4.1}$$

where y is the transverse deflection, z is the axial coordinate, E is Young's modulus, ρ is the mass density, and $I = \pi a^4/4$ is the second moment of area for a fiber of cross-sectional area A. For small deflections $|y/a|^2 \ll 1$, the local moment may be expressed as

$$M(z, t) = EI \frac{\partial^2 y}{\partial z^2}. \tag{4.2}$$

The condition for validity of (4.1) is [10]

$$af_F/v_t < 0.1 \tag{4.3}$$

where $f_F \sim 17$ MHz and $v_t = 3764$ m/s, the shear velocity in silica. In the reported experiment [1], this parameter has the value 0.28, which places the waves in the transition regime between low- and high-frequency waves [10] and has implications for the overlap of acoustic and optical power; at higher frequencies, the acoustic energy shifts from a bulk flexural disturbance to an acoustic surface wave, thus reducing its influence on the guided modes. Under these conditions, the actual overlap integral will therefore be somewhat smaller than Q. A useful additional quantitative correction may be made by carefully distinguishing the group from the phase velocity and replacing them with accurate values from the more complete theory [10].

The phase velocity of the flexural waves described by (4.1) is

$$v_F^2 = \frac{EIK^2}{\rho A} = (\pi a v_o/\Lambda_F)^2 \tag{4.4}$$

where $v_0 = \sqrt{(E/\rho)}$ is the extensional wave phase velocity (5760 m/s in silica). The general relationship for the group velocity of dispersive waves is

$$v_{gF} = \left\{ v_F \Big/ \left(1 - \frac{\Omega}{v_F} \frac{\partial v_F}{\partial \Omega} \right) \right\} \tag{4.5}$$

and it may be used to show that for low-frequency flexural waves, $v_{gF} = 2v_F$. Using $\partial^2/\partial t^2 = -\Omega^2$ in (4.1) and substituting (4.2) yields

$$M(z, t) - \frac{1}{K^4} \frac{\partial^4 M}{\partial z^4} = M_d(z, t) \tag{4.6}$$

where the driving term M_d has been incorporated (3.6). Expressing the moment wave as

$$M(z, t) = \tfrac{1}{2} A_F(z) \exp \{-j(Kz - \Omega t)\} + \text{c.c.} \tag{4.7}$$

where $A_F(z)$ is its slowly varying amplitude, substituting $M(z, t)$ into (4.6), neglecting all but first-order spatial derivatives of A_F, and collecting coefficients of $\exp \{-j(Kz - \Omega t)\}$ yields

$$\pm \frac{\partial A_F}{\partial z} + \frac{\alpha_F}{2} A_F = -j \frac{\Omega a}{4 v_{gF}} \left\{ \epsilon_o Q A_{eq} \frac{\partial \epsilon_r}{\partial s} \right\} A_B^* A_L \tag{4.8}$$

where the expression in (3.6) has been substituted for M_d and a phenomenological absorption α_F m^{-1} is incorporated. This absorption is related to the phonon lifetime τ_F and bandwidth Δf_F by $\alpha_F = \Delta f_F/v_F = 1/v_F\tau_F$. The upper sign is chosen if the acoustic wave copropagates with the optical waves, i.e., if the pump light is launched into the LP_{01} mode.

V. Intermodal Coupling by Flexural Microbending

It is straightforward to show that the mechanical strain s due to the presence of a low-amplitude flexural wave is

$$s = r \cos \phi \frac{\partial^2 y}{\partial z^2} = \frac{r \cos \phi}{EI} M(z, t). \tag{5.1}$$

Using (3.3), one can translate s into a change in ϵ_r:

$$\Delta \epsilon_r(r, \phi, z) = \frac{\partial \epsilon_r}{\partial s} \frac{r \cos \phi}{2\, EI} A_F(z) \cdot \exp \{-j(Kz - \Omega t)\} + \text{c.c.} \tag{5.2}$$

Incorporating $\Delta \epsilon_r$ in Maxwell's equations for the fiber modes and carrying out a standard coupled-wave analysis yields, with some rearrangement,

$$\frac{\partial A_B}{\partial z} + \frac{\alpha}{2} A_B = -j \frac{\omega_B a}{4 v_{gB}} \left\{ \frac{Q}{EIn_B^2} \frac{\partial \epsilon_r}{\partial s} \right\} A_F^* A_L \tag{5.3}$$

and

$$\frac{\partial A_L}{\partial z} + \frac{\alpha}{2} A_L = -j \frac{\omega_L a}{4 v_{gL}} \left\{ \frac{Q}{EIn_L^2} \frac{\partial \epsilon_r}{\partial s} \right\} A_F A_B \tag{5.4}$$

where, once again, a phenomenological optical absorption α per meter has been added. The optical group velocities v_{gB} and v_{gL} arise from a more accurate treatment of the guided modes; they are distinguished from the phase velocities c/n_L and c/n_B (which they closely equal) for clarity. The FSBS process is now described by (4.8), (5.3), and (5.4). For full benefit, it is necessary to normalize the amplitudes A_B, A_L, and A_F to the total power involved in the parametric process.

VI. Power-Normalized Coupled-Wave Equations for FSBS

The power density in any guided wave is given by the average energy stored per unit volume (W) multiplied by the group velocity. For flexural waves, this leads to a total power of

$$P_F = \left[\frac{1}{2EI} |A_F|^2 \right] v_{gF} = \left[\frac{2\pi f_F^2}{a^2 \rho v_F^4} |A_F|^2 \right] v_{gF}. \tag{6.1}$$

In the case of pump and Brillouin modes, the equivalent expressions are

$$P_L = \left[\frac{A_{eq} n_L^2 \epsilon_o}{2} |A_L|^2 \right] v_{gL}$$

and

$$P_B = \left[\frac{A_{eq} n_B^2 \epsilon_o}{2} |A_B|^2 \right] v_{gB}. \tag{6.2}$$

Defining the normalized amplitudes a_L, a_B, and a_F as

$$a_m = \sqrt{(P_m/P_{tot})} \tag{6.3}$$

where $m = L$, B, or s and P_{tot} is the total incident power, the three coupled amplitude equations (4.8), (5.3), and (5.4) may be reexpressed in normalized form as follows:

$$\frac{\partial a_L}{\partial z} + \frac{\alpha}{2} a_L = -j\kappa_L a_F a_B \tag{6.4a}$$

$$\frac{\partial a_B}{\partial z} + \frac{\alpha}{2} a_B = -j\kappa_B a_F^* a_L \tag{6.4b}$$

$$\pm \frac{\partial a_F}{\partial z} + \frac{\alpha_F}{2} a_F = -j\kappa_F a_L a_B^* \tag{6.4c}$$

where the upper sign is taken if the flexural wave copropagates with the laser and Brillouin waves, and the lower sign if it counterpropagates. If the laser is launched into the LP_{01} mode, the upper sign holds. The coupling constants are defined by

$$\kappa_L = \omega_L/C_F, \qquad \kappa_B = \omega_B/C_F,$$
$$\kappa_F = \Omega/C_F \tag{6.5}$$

and the velocity C_F is given by the expression

$$C_F = \frac{n_L n_B}{Q(\partial \epsilon_r/\partial s)} \sqrt{\left\{\frac{2\pi v_{gL} v_{gB} v_{gF} E a^2}{P_{tot}}\right\}}. \tag{6.6}$$

The approximations $v_{gL} \approx c/n_L$ and $v_{gB} \approx c/n_B$ are valid in these expressions. The energy conservation equation (2.1) yields the result that

$$\kappa_L - \kappa_F - \kappa_B = 0, \tag{6.7}$$

which, in turn, may be used to demonstrate that solutions of (6.4) conserve power.

VII. Solutions and Brillouin Gain

Equation (6.4) may be recast in a mathematically more elegant form if each of the complex amplitudes is expressed in terms of the real-valued quantities b_m and ϕ_m:

$$a_m = b_m \exp(j\phi_m)$$

where m is L, B, or S. After some manipulation, it is found that

$$b_L b_B b_F \cos\psi = B_o \exp\{-(\alpha \pm \alpha_F/2)z\} \tag{7.1}$$

where B_o is set by the boundary conditions. Power conservation is expressed by the equation

$$\frac{\partial}{\partial z}(p_L + p_B \pm p_F) + \alpha(p_L + p_B) + \alpha_F p_F = 0 \tag{7.2}$$

where $p_m = b_m^2$ is the normalized power in wave m. Finally, the coupled-wave equation set becomes

$$\frac{\partial p_L}{\partial z} + \alpha p_L = -2\kappa_L b_L b_F b_B \sin\psi$$

$$\frac{\partial p_B}{\partial z} + \alpha p_B = 2\kappa_B b_L b_F b_B \sin\psi$$

$$\pm \frac{\partial p_F}{\partial z} + \alpha_F p_F = 2\kappa_F b_L b_F b_B \sin\psi \tag{7.3}$$

where

$$\psi = (\phi_L - \phi_B - \phi_F) \tag{7.4}$$

is the relative phase and the + sign refers to the case where the flexural wave copropagates with the light.

The boundary condition at $z = 0$ must be such that all the waves carry finite power, although, of course, the pump will, in general, overwhelmingly dominate. The maximum parametric gain is experienced when the relative phase at $z = 0$ is $\psi = \pi/2$ (power flow $p_L \rightarrow p_B$) or $3\pi/2$ ($p_B \rightarrow p_L$), which yields, from (7.1), $B_o = 0$. This is the case of interest in FSBS since Brillouin and flexural waves satisfying this phase relationship will reach threshold first. From this point on, therefore, $B_o = 0$ is assumed, which implies that ψ remains at $\pi/2$ or $3\pi/2$ throughout the interaction (because the product $b_L b_B b_F$ is zero only under very special conditions).

Although (7.3) may be numerically solved (this is easier when all three waves copropagate), it is instructive to follow the precedent set in many backward SBS analyses [13], and to treat the special case when $\partial p_F/\partial z$ is negligible. For validity, this implies that the characteristic phonon absorption length $1/\alpha_F$ must be smaller than the characteristic length for the FSBS process $1/g_{BF}$. This is a good approximation in backward SBS; however, this is not necessarily true in FSBS, as we shall see. Adopting it for the present, the following differential equation pair may be obtained:

$$\partial p_B/\partial z = \{-\alpha + g_{BF} p_L\} p_B$$
$$\partial p_L/\partial z = \{-\alpha - g_{BF} p_B\} p_L \tag{7.5}$$

where the Brillouin gain g_{BF} m^{-1} is

$$g_{BF} = (4\kappa_B \kappa_F/\alpha_F) \tag{7.6}$$

and $\kappa_L \approx \kappa_B$ is used. The general solution of these equations is

$$p_B(z) = p_{B0}\left\{\frac{(p_{L0} + p_{B0})\exp(-\alpha z)}{p_{B0} + p_{L0}\exp\{-g_{BF}(p_{B0} + p_{L0})L_i\}}\right\} \tag{7.7}$$

where $p_L(z) = \{(p_{B0} + p_{L0})\exp(-\alpha z) - p_B(z)\}$ and the effective interaction length

$$L_i = \{1 - \exp(-\alpha z)\}/\alpha. \tag{7.8}$$

The quantities p_{B0} and p_{L0} are the initial values of p_B and p_L at $z = 0$. If pump depletion due to FSBS is neglected, the solution becomes

$$p_B(z) = p_{B0}\exp\{-\alpha z + g_{BF} L_i\} \tag{7.9}$$

which is formally identical to the expression commonly derived in backward SBS, and which makes no distinction as to whether the flexural wave is co- or counterpropagating.

In order to compare the gains in FSBS to those in BSBS, it is necessary to derive the coupling constants for the backward SBS interaction. They take a form similar to (6.5), the only difference being in the definition of C_F, which becomes

$$C_o = \frac{n_L n_B}{\partial \epsilon_r/\partial s} \sqrt{\left\{\frac{8 v_{gL} v_{gB} v_{go} E A_{eq}}{P_{tot}}\right\}} \tag{7.10}$$

where a subscript "o" is used to signify backward SBS, and otherwise all of the parameters have the same meanings.

It is now possible to obtain an expression for the ratio of g_{BF} to the Brillouin gain at the same power level in backward SBS, g_{Bo}:

$$g_{BF}/g_{Bo} = \frac{\alpha_o f_F v_{go}}{\alpha_F f_o v_{gF}}\left[\frac{2Qr_{eq}}{a}\right]^2 \approx \frac{\alpha_o \Lambda_o}{2\alpha_F \Lambda_F}\left[\frac{r_{eq}}{a}\right]^4 \tag{7.11}$$

where $Q \approx r_{eq}/2a$ has been used. The reasons for this strong dependence on r_{eq}/a are that 1) the acoustic power is distrib-

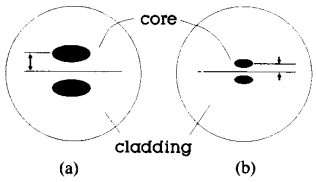

Fig. 4. The electrostrictive moment arm for two different spot diameters in a fiber of constant cladding radius. Because the axial electrostrictive force depends only on the optical power, it is advantageous (at a fixed total optical power) to have an optical spot size as large as possible, in contrast to every other known nonlinear effect. This is because the axial electrostrictive force is independent of the area of the elliptical regions, whereas the resulting moment is proportional to the moment arm (marked).

uted over the entire fiber cross section, while the optical power is concentrated in the core, and 2) the induced electrostrictive moment scales with r_{eq}. Point 2) is further clarified by noting that the axial electrostrictive force (pressure × area) depends only on the optical power, whatever its intensity; enlarging the spot size yields a higher moment since the moment arm lengthens while the electrostrictive force remains unchanged (see Fig. 4). The consequence is that, in peculiar contrast to all other nonlinear effects, larger spot sizes of the optical mode increase the nonlinearity ($r_{eq} \leq a$).

VIII. Discussion

A. Brillouin Gain

Explicit expressions for the Brillouin gain in units for m/W (denoted $\bar{g}_{BF}$ and $\bar{g}_{Bo}$) take the forms

$$\bar{g}_{BF} = G_B \left\{ \frac{(r_{eq}/a)^4}{\Lambda_F \alpha_F} \right\} \tag{8.1}$$

and

$$\bar{g}_{Bo} = G_B \left\{ \frac{2}{\Lambda_o \alpha_o} \right\} \tag{8.2}$$

where

$$G_B = \frac{(\pi \partial \epsilon_r / \partial s)^2}{\lambda_B c n_L n_B E}. \tag{8.3}$$

In the experiment recently reported [1], $\lambda_B = 514.5$ nm and $E = 73$ kN · mm^{-2}, yielding $G_B = 4.5 \times 10^{-12}$ m/W. Graphs of $\bar{g}_{BF}$ versus r_{eq}/a for various values of α_F are plotted in Fig. 5 for $L_b = \Lambda_F = 0.17$ mm and $r_{eq} = 2.3$ μm. For comparison, $\bar{g}_{Bo}$ at $\Lambda_o = \lambda_B/2n = 176$ nm and $\alpha_o = 10^6$ m^{-1} is also plotted. Large values of r_{eq}/a significantly favor FSBS. If r_{eq} is varied, keeping a constant, a similar result is obtained, although the beat length $L_b = \Lambda_F$ at constant normalized frequency V (chosen to lie in the dual-mode regime $2.405 < V < 3.832$) will scale linearly with r_{eq} and reduce the quartic dependence on r_{eq} to cubic. Even so, under these circumstances, increasing the spot size at constant pump power will still lower the FSBS threshold. The flexural phase velocity and frequency, together with the parameter af_F/v_t from (4.3), are plotted in Fig. 6 for the same case as in Fig. 5. The limits of validity of the low-frequency flexural wave approximation are marked. The experiment in [1] lies in the shaded region. Taking an acoustic loss α_F of around 1 m^{-1}, the ratio of forward to backward Brillouin gain is on the order of 10^{-2}.

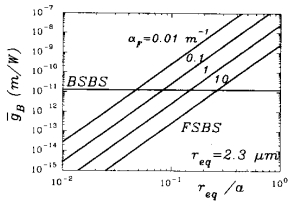

Fig. 5. Brillouin gains in meters/watt plotted against the ratio of modal to cladding radii at different levels of flexural-wave absorption α_F. The parameter values were $\Lambda_F = 0.17$ mm and $r_{eq} = 2.3$ μm. The equivalent BSBS gain is included for comparison.

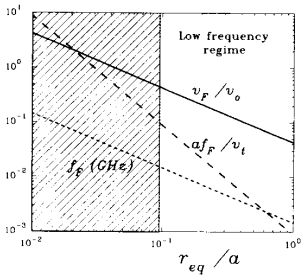

Fig. 6. Various parameters plotted against r_{eq}/a for the FSBS case in Fig. 5. The analysis is valid in the low-frequency region where [from (4.3)] the parameter $(af_F/v_t) \leq 0.1$.

B. Numerical Solutions

Numerical solutions allow treatment of the case, clearly of importance in FSBS, when it is no longer valid to neglect $\partial p_F/\partial z$. This will happen if the acoustic loss is small compared to the Brillouin gain, i.e., when $\alpha_F/g_{BF} \ll 1$. The consequence of an increased phonon lifetime is that an acoustic wave excited in one part of the fiber may travel a significant distance without serious absorption to another section of fiber where the relative phase ψ is different. Graphs of the z dependence of p_F, p_B, and p_L for a series of transition cases are plotted in Fig. 7. The traveling optical interference fringes that provide gain via electrostriction for the flexural wave in one section of fiber flip their phase by 180° at the transition between one coupling cycle and the next (see Fig. 8 for a logarithmic plot of the case in Fig. 7(c), including the acoustic-wave power p_F). An acoustic wave that travels over this transition will immediately experience negative electrostrictive gain and begin to lose power, donating energy to the Brillouin signal, which is then up-converted back to the pump frequency. As the parameter α_F/g_{BF} falls in magnitude, the number of possible coupling cycles rises. As it rises in value, the solution (7.7) is approached when frequency up-conversion of the Brillouin signal is impossible since the acoustic phonons are absorbed almost immediately after being created; they do not then travel far enough to experience the flip in phase just mentioned. Under these conditions, it is expected that the approximate solution in (7.7) will become valid. To provide confirmation of this, the accurate and approximate solutions are compared in Fig. 9; (7.7) predicts a premature onset of the stimulated Brillouin process, somewhat nearer the launch end than is correct. Otherwise, the behavior is very similar. The initial value of p_B was set arbitrarily to 10^{-9} for these calculations, $p_F(0)$ was set equal to

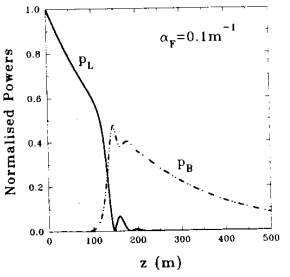

(a)

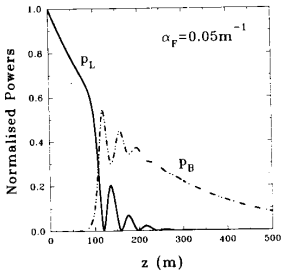

(b)

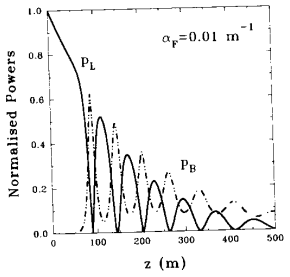

(c)

Fig. 7. Growth of FSBS with distance, calculated by numerical integration of (7.3) at three different values of acoustic loss: (a) 0.1 m^{-1}, (b) 0.05 m^{-1}, and (c) 0.01 m^{-1}. The other parameter values are P_{tot} = 200 mW, an optical wavelength of 514.5 nm, r_{eq} = 5 μm, a = 25 μm, and α = 0.005 m^{-1}, giving v_F = 1330 m/s and f_F = 3.9 MHz. The Brillouin gain in each case is (a) 0.54 m^{-1}, (b) 1.1 m^{-1}, and (c) 5.4 m^{-1}. See the text for a more detailed interpretation.

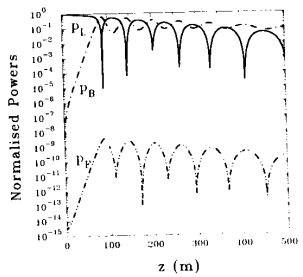

Fig. 8. Plot in Fig. 7(c) rescaled logarithmically and including the flexural-wave power p_F. The complex interdependence of the three parametrically coupled waves is clear (see text).

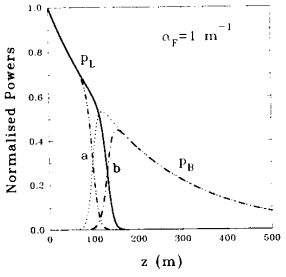

Fig. 9. Comparison of (a) the approximate solution (7.7) to (b) that resulting from numerical integration of (7.3). The other parameter values are the same as in Fig. 7, with the exception that the power level is 1 W and g_{BF} = 0.27 m^{-1}. The approximate solution underestimates the interaction length needed before the FSBS signal becomes significant.

$\{(2\kappa_F/\alpha_F)^2 p_{B0} p_{L0}\}$, and ψ was set equal either to $\pi/2$ or $3\pi/2$, depending on the position in the coupling cycle.

C. Thresholds for BSBS and FSBS

Following Smith [14], the spontaneous Brillouin signal (caused by the scattering of pump light at thermally excited acoustic phonons) can be incorporated into (7.5) as follows:

$$\partial p_B/\partial z = -\alpha p_B + g_{BF} p_L \{p_B + s_B\}$$
$$\partial p_L/\partial z = -\alpha p_L - g_{BF} p_L \{p_B + s_B\} \tag{8.4}$$

where the normalized spontaneous Brillouin power s_B is given by

$$s_B = \frac{\nu_B \Delta\nu_L kT}{f_F P_{tot}} \approx \frac{\nu_L \Delta\nu_L kT}{f_F P_{tot}} \tag{8.5}$$

and k is Boltzmann's constant. As before, these equations are valid only if $\alpha_F \gg g_{BF}$. Although (8.4) may be numerically integrated, the threshold power can be found by neglecting nonlinear pump depletion, i.e., setting $p_L(z) = \exp(-\alpha z)$, and integrating the first equation labeled (8.4). This yields

$$p_B(z) = (s_B g_{BF}/\alpha) \exp(-\alpha z) \int_0^Y \frac{\exp(g_{BF} y/\alpha)}{y + \exp(-\alpha z)}\, dy \tag{8.6}$$

where $Y = 1 - \exp(-\alpha z)$. Making the approximation that the integrand is significant only in the range where $y \approx 1$ (assuming that the fiber is long enough to allow $\exp(-\alpha z) \ll 1$), (8.6) may then be integrated. Following Smith in defining the threshold as occurring when the Brillouin signal equals $p_L(z) = \exp(-\alpha z)$, the threshold power P_{th} is a solution of

$$P_{th} = (\nu_L \Delta\nu_L kT/f_F) \exp\{\bar{g}_{BF} P_{th} L_i/\pi r_{eq}^2\} \tag{8.7}$$

where the exponential function is assumed to be much greater than 1. This shows that the growth from noise can be approximately modeled by means of an equivalent injected Brillouin power $P_{BF}(0) = (\nu_L \Delta\nu_L kT/f_F)$ at $z = 0$, which corresponds to an injected photon flux of kT/hf_F per mode within the pump laser linewidth. The equivalent BSBS signal is usually considered to be injected at the point in the fiber where the local Brillouin gain is exactly balanced by the optical loss [14]; since, in our case, this point mostly lies beyond the fiber length, we set it at $z = L$. The equivalent injected power at $z = L$ is $P_{Bo}(L) = (\nu_L \Delta\nu_L kT/f_o)$, which leads to an equation analogous to (8.3):

$$P_{th} = (\nu_L \Delta\nu_L kT/f_o) \exp\{\bar{g}_{Bo} P_{th} L_i/\pi r_{eq}^2\}. \tag{8.8}$$

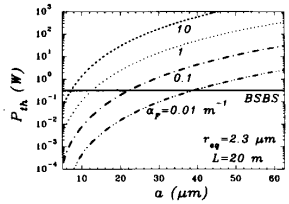

Fig. 10. Threshold pump power levels in FSBS and BSBS for different values of α_F plotted against the cladding radius a at constant mode spot size $r_{eq} = 2.3$ μm. Refer to the text for more details.

For a laser linewidth $\Delta\nu_L = 25$ MHz, $\lambda_L = 514.5$ nm, $T = 293°C$, $f_F = 17$ MHz, and $f_o = 32$ GHz, the equivalent injected powers turn out to be $P_{BF}(0) = 3.5$ μW and $P_{Bo}(L) = 1.8$ nW.

Computed threshold power levels, obtained by iteratively solving (8.7) and (8.8), are presented in Fig. 10 as a function of a, the cladding radius, for $\alpha = 20$ dB/km, $\alpha_o = 10^6$/m, $r_{eq} = 2.3$ μm, $L = 20$ m, and $L_f = 0.17$ mm. The acoustic flexural-wave loss α_F is varied as a parameter, and account is taken of the variation of f_F with a. As expected, smaller values of a significantly favor FSBS. In the reported experiment [1], a much lower threshold for FSBS than predicted by Fig. 10 was found. The implications of this will require further careful experimental study.

Since FSBS does not require a long laser coherence length (the Brillouin and pump waves copropagate, and are therefore closely correlated), the use of a multifrequency laser line will suppress the BSBS signal in favor of the FSBS.

IX. Conclusions

It is emphasized that the analysis presented is fully valid only in the low-frequency flexural-wave regime where the inequality in (4.3) holds. It will remain qualitatively valid outside this regime, however, with somewhat reduced values of acoustic/optical overlap, and hence Brillouin gain. Within this restriction, the FSBS gain can be greatly enhanced by appropriate fiber design and by employing a laser running single line, but multifrequency. It varies as $(r_{eq}/a)^4$, and hence, it is improved (at constant pump power) for larger modal spot sizes. FSBS is thus unique in being the only known nonlinear effect which is enhanced by reducing the optical intensity while keeping the power constant. This odd behavior arises because 1) the axial electrostrictive force is independent of the spot radius r_{eq}, and 2) its moment arm increases with r_{eq}. The standard approximation used in BSBS—that the acoustic absorption length is much shorter than the Brillouin gain length—is no longer always valid in FSBS. The consequence is that nonlocalized acoustic-wave coupling in both directions between the pump and the Brillouin modes can take place. Within the effective interaction length L_i, many cycles of coupling can take place. Experiments remain to be done on specially designed fibers with 1) plastic coating removed to reduce α_F, 2) large dual-mode spot sizes (requires a small core/cladding refractive index step), and 3) large values of r_{eq}/a. Attention to these details will greatly reduce the FSBS threshold power level. For example, a fiber with a mode spot radius of 10 μm and an outer radius of 25 μm would have a beat period of around 0.7 mm, an FSBS shift of around 1 MHz ($v_F = 646$ m/s), and a Brillouin gain of 1.6×10^{-8} m/W for $\alpha_F = 0.01$ m^{-1}. In the same fiber, the BSBS gain is 5.3×10^{-11} m/W, some three orders of magnitude smaller. The FSBS gain would then be a factor of 3×10^5 greater than under the recorded experimental conditions [1].

References

[1] P. St. J. Russell, D. Culverhouse, and F. Farahi, "Experimental observation of forward stimulated Brillouin scattering in dual-mode single-core fibre," *Electron. Lett.*, vol. 26, pp. 1195–1196, 1990.
[2] R. M. Shelby, M. D. Levenson, and P. W. Bayer, "Guided acoustic wave Brillouin scattering," *Phys. Rev.*, vol. B31, pp. 5244–5252, 1985.
[3] S. R. Friberg, Y. Silberberg, M. K. Oliver, M. J. Andrejco, M. A. Saifi, and P. W. Smith, "Ultra-fast all-optical switching in dual-core fiber nonlinear coupler," *Appl. Phys. Lett.*, vol. 51, pp. 1135–1137, 1987.
[4] S. Trillo, S. Wabnitz, R. H. Stolen, G. Assanto, G. I. Stegeman, and C. T. Seaton, "Experimental observation of polarisation instability in a birefringent optical fiber," *Appl. Phys. Lett.*, vol. 49, pp. 1224–1226, 1986.
[5] S. Trillo, S. Wabnitz, and G. I. Stegeman, "Nonlinear codirectional guided wave mode conversion in grating structures," *J. Lightwave Technol.*, vol. 6, pp. 971–976, 1988.
[6] P. St. J. Russell and D. N. Payne, "Nonlinear switching in strongly coupled periodic dual waveguide couplers," presented at the Top. Meet. Nonlin. Guided-Wave Phenom.: Phys. and Appl., Houston, TX, 1989, paper FC2-1.
[7] B. Y. Kim, J. N. Blake, H. E. Engan, and H. J. Shaw, "All-fiber acoustooptic frequency shifter," *Opt. Lett.*, vol. 11, pp. 389–391, 1986.
[8] J. N. Blake, B. Y. Kim, H. E. Engan, and H. J. Shaw, "Analysis of intermodal coupling in two-mode fiber with periodic microbends," *Opt. Lett.*, vol. 12, pp. 281–283, 1987.
[9] H. Sabert, L. Dong, and P. St. J. Russell, "In-line flexural wave optical modulator, filter and frequency shifter in dual-core fibre," presented at the Topical Meet. Integrated Photon. Res., Hilton Head, SC, Mar. 1990, paper TuD9.
[10] H. E. Engan, B. Y. Kim, J. N. Blake, and H. J. Shaw, "Propagation and optical interaction of guided acoustic waves in two-mode optical fibers," *J. Lightwave Technol.*, vol. 6, pp. 428–436, 1988.
[11] See L. D. Landau and E. M. Lifshitz, *Electrodynamics of Continuous Media, Course of Theoretical Physics, Vol. 8.* Oxford: Pergamon, 1963.
[12] R. N. Thurston, "Elastic waves in rods and clad rods," *J. Acoust. Soc. Amer.*, vol. 64, pp. 1–37, 1978.
[13] For analysis of backward SBS, see Y. R. Shen, *The Principles of Nonlinear Optics.* New York: Wiley-Interscience, 1984, p. 189.
[14] R. G. Smith, "Optical power handling capacity of low loss optical fibers as determined by stimulated Raman and Brillouin scattering," *Appl. Opt.*, vol. 11, pp. 2489–2494, 1972.

P. St. J. Russell, photograph and biography not available at the time of publication.

D. Culverhouse, photograph and biography not available at the time of publication.

F. Farahi, photograph and biography not available at the time of publication.